

CO₂ Surface Variability, from the Stratosphere or Not?

Michael J. Prather

5 Earth System Science Department, University of California Irvine, Irvine CA 92617 USA

Correspondence to: Michael J. Prather (mprather@uci.edu)

Abstract. Fluctuations in atmospheric CO₂ can be measured with great precision and are used to identify
10 human-driven sources as well as natural cycles of ocean and land carbon. One source of variability is the
stratosphere, where the influx of aged CO₂-depleted air can produce fluctuations at the surface. This
process has been speculated a potential source of interannual variability (IAV) in CO₂ that might obscure
the quantification of other sources of IAV. Given the recent success in demonstrating that the
stratospheric influx of N₂O- and chlorofluorocarbon-depleted air is a dominant source of their surface
15 IAV in the southern hemisphere, we here apply the same model and measurement analysis to CO₂. Using
chemistry-transport modeling or scaling of the observed N₂O variability, we find that the stratosphere-
driven surface variability in CO₂ is at most 10% of the observed IAV and is not an important source.
Diagnosing the amplitude of the CO₂ annual cycle and its increase from 1985 to 2021 through the annual
variance gives rates similar to traditional methods in the northern hemisphere (BRW, MLO), but can
20 identify the emergence of small trends (0.08 ppm decade⁻¹) in the southern hemisphere (SMO, CGO).

1 Introduction

The surface abundance of CO₂, a.k.a. the Keeling Curve (Figure 1a), is used as the prime example of the
25 human-driven increases in greenhouse gases. It is also used to demonstrate control of CO₂ by the land
biosphere and the oceans through its annual cycles and interannual variations (Le Quéré et al., 2016;
2018). The inverse modeling of surface sources based on these CO₂ observations is used to infer regional
sources of fossil fuel emissions as well as year-to-year changes in primary productivity of the biosphere
or oceanic degassing (e.g., Gurney et al., 2002; Baker et al., 2006; Engelen et al., 2006; Nassar et al.,
30 2011; Peylin et al., 2013; Frankenberg et al., 2016; Pandey et al., 2016; Nakazawa, 2020). There is
concern that atmospheric variations in CO₂, and hence the net sources derived from them, may be affected
by interannual variations (IAV) in tropospheric mixing or stratosphere–troposphere exchange (STE)
(Gaubert et al., 2019), but there are no definitive studies. For example, Nazakawa's (2020) review of
greenhouse gas studies mentions the stratosphere only in connection with CH₄ and N₂O, not with CO₂.

35 The possibility of a true STE-driven IAV CO₂ signal, raised by Gaubert et al. (2019), has not been
seriously investigated. For the most part, when studies investigate the stratospheric influence on CO₂
source inversions, they are not concerned about STE fluxes directly but other factors that degrade the
results: e.g., gradients across the tropopause, the effective tropospheric air mass diluting surface
40 emissions, or the inclusion of CO₂-depleted stratospheric air in column CO₂ calculations (Nassar et al.,
2011; Deng et al., 2015; Frankenberg et al., 2016; Pandey et al., 2016). For example, Le Quéré et al.
(2018) are concerned how emissions will mix throughout the troposphere and the stratosphere, but not
how stratospheric air will come back down to the surface. Only studies of the CO₂ triple-oxygen isotope
signature ($\Delta^{17}\text{O}$) are concerned with accurate STE fluxes, recognizing its importance in the seasonal
45 isotopic signals (Liang et al., 2017; Koren et al., 2019; Laskar et al., 2019).

Both models and observations have shown that the stratospheric quasi-biennial oscillation (QBO) modulates the STE and drives much of the IAV observed in surface N₂O through the stratospheric influx of N₂O-depleted air (Hamilton and Fan, 2000; Nevison et al., 2004; 2011; Ray et al., 2020; Ruiz et al., 2021; Ruiz and Prather, 2022). Here, we use the N₂O studies of Ruiz et al. (2021) with parallel model simulations of CO₂ to place constraints on the CO₂ IAV caused by atmospheric circulation, finding that this effect is a clear but minor perturbation in driving the observed IAV of CO₂.

2 Methods and Analysis

We investigate the CO₂ IAV and its causes using surface CO₂ observations from 1985 through 2020, surface N₂O observations from 1997 through 2020, and tracer simulations from the UC Irvine chemistry-transport model (CTM) simulations for the historical period 1990-2017.

To study the circulation-driven IAV of CO₂, including STE, we focus on the southern hemisphere (SH) because fluctuations in the large biosphere-driven seasonality in the northern hemisphere (NH) (Figure 1a) will obscure any stratosphere-driven IAV there. The UCI CTM uses ECMWF Integrated Forecast Fields at 1.1° horizontal resolution and has proven quite successful in simulating the historical IAV of surface N₂O, ozone columns, and the Antarctic ozone hole (Ruiz et al., 2021; Ruiz and Prather, 2021; Tang et al., 2021). For CO₂, we develop two model scenarios to highlight the impacts of atmospheric transport. First, we define a surface emissions-driven eCO₂ scenario, in which the total atmosphere increases at a constant rate of 2 ppm (parts per million, dry-air mole fraction) y⁻¹, driving a flux of about 2 PgC y⁻¹ into the SH. This eCO₂ scenario is a simple experiment with area-uniform (20° N – 60° N) and time-constant emissions to test how atmospheric circulation driving a NH-SH gradient might affect the seasonal and interannual variability of SH surface CO₂. It is obviously not realistic, lacking the large biospheric and oceanic seasonality. A second, stratospheric-driven, sCO₂ scenario, is forced with a net stratospheric flux of CO₂-depleted air being transported into the troposphere and down to the surface. This STE flux is calculated as the equivalent of the aging of stratospheric CO₂ relative to the troposphere (2 ppm y⁻¹), yielding an apparent negative CO₂ flux of about 0.4 PgC y⁻¹ into each hemisphere. This forcing flux is placed in the uppermost model layer (~80 km altitude) and transported to the surface. In both of these cases, CO₂ is changing linearly with a known trend, and we subtract that trend to get the modeled anomalies. The eCO₂ scenario effectively forces the stratosphere with a negative flux of 2 ppm y⁻¹, but most of the SH signal comes from the much larger interhemispheric flux. A third, independent method for deriving CO₂ IAV uses the observed SH surface N₂O signal, driven by stratospheric photochemical loss of 13 TgN (as N₂O) y⁻¹, as a measure of STE influence. In this case we scale the results to CO₂ using the ratio of the STE fluxes, i.e., 0.15 ppm CO₂ per ppb N₂O. Ruiz et al. (2021, Figures 3 and S3) show that the tropospheric QBO patterns for N₂O and CFC1₃ are nearly identical despite the different vertical locations and QBO patterns in their stratospheric loss. A species STE flux pattern (i) scales with the total flux out of the stratosphere and (ii) is determined by the dynamics of the lowermost mid-latitude stratosphere (Ruiz and Prather, 2022, Figure 1).

The monthly CO₂ surface observations are gathered from NOAA ESRL (Dlugokencky et al., 2021a). We use 5 sites: BRW = Barrow AK, 71° N, 156° W; MLO = Mauna Loa HI, 20° N, 156° W; SMO = Tutuila, Am. Samoa, 14° S, 171° W; CGO = Cape Grim, Tasmania, Australia, 41° S, 144° E; and SPO = South Pole, 90° S. Monthly average in situ observations are used, and gaps are filled by flask data at the same site. CGO is flask only. We have a continuous monthly record from 1985 through 2020 (Figure 1a). We

convert these to a stationary series of residuals by fitting polynomials, assuming the months are equally spaced. The 2nd, 3rd, 4th, and 5th order polynomials produce almost identical results for each site (not shown), and the average 3rd and 4th order fits are subtracted to calculate the residuals. The CO₂ residuals for the average of SPO+CGO are shown in Figure 1c as the red line, which shows a clear annual cycle plus equally large variability on decadal scales. The annual cycle of CO₂ and its rate of change is a critical metric used to evaluate the carbon cycle in Earth system models (Graven et al., 2013; Zhao and Zeng, 2014; Wenzel et al., 2016). Here, we calculate the cycle simply by averaging each calendar month of the year, with results shown in Figure 1b. The annual amplitudes (max-min) are 16.4, 6.4, 0.92, 1.02, and 1.14 ppm for BRW, MLO, SMO, CGO, and SPO, respectively. These are consistent with those previous studies, although SH cycles remain understudied and not well evaluated. In some months SMO at 14°S can be north of the South Pacific Convergence Zone and thus influenced by NH air, explaining its non-sinusoidal cycle when compared with SPO and CGO. Also shown is the annual cycle for the modeled eCO₂ scenario (~0.18 ppm, dotted lines for SMO and SPO). That for the sCO₂ scenario is even smaller (~0.06 ppm) and is not shown. It is interesting that the SH annual cycles in eCO₂ are similar in shape to those observed, even catching the double peak at SMO, but the magnitude is much smaller. There is no evidence in our direct modeling or analysis that stratosphere-troposphere exchange, which does drive an annual cycle in N₂O, can produce a detectable annual cycle in CO₂ above the large observed cycle.

The observed QBO signal in surface N₂O (Ruiz et al., 2021, Figure 3) has largest amplitude in the SH extra-tropics, becoming weaker in the tropics and NH. Because this signal is nearly uniform across the SH extra-tropics in both observations and models, we combine the SPO and CGO CO₂ data and focus our efforts on that time series. The challenge is to extract the CO₂ IAV signal in the 2–5 year period range. A simple 12-month running mean is great for removing the annual cycle, but leaves the large amplitude decadal periods (blue dashed line in Figure 1c). We select band-pass filtering, while recognizing that this method can produce spurious results, especially at the edges. After several false starts, and with help from the reviewers, we chose the matlab *bandpass()* filter. This function is well documented (www.mathworks.com/help/signal/ref/bandpass.html), and the band pass is defined by the lower and upper cut-off frequencies. After experimentation with the CO₂ signal to reduce edge effects, we chose the following settings: band pass frequency (y⁻¹) range [0.20 0.80]; *bandpass* applied forward and backward is averaged; *ImpulseResponse* = iir; *Steepness* = 0.85. A wider filter, e.g., [0.16 0.95], produced similar results for the middle years, but large swings for the beginning and end years. IAV signals derived from frequency filtering for the last 2-3 years of the record are not robust. The resulting band-pass IAV (thick black line in Figure 1c) clearly shows the patterns seen in the 12-month running mean. The SMO IAV is calculated in the same way and plotted alongside the SPO+CGO IAV in Figure 1d. The IAV for N₂O observations and the modeled eCO₂ and sCO₂ scenarios use the same processing.

For monthly N₂O surface observations, also from NOAA ESRL (Dlugokencky et al., 2021b), we focus on SH extra-tropics, using SPO, CGO, plus 3 other sites: S30 = Western Pacific Cruise, 30° S, 168° E; USH = Tierra del Fuego, Ushuaia, Argentina, 55° S, 68° W; and PSA = Palmer Station, Antarctica, 65° S, 64° W. All five sites have nearly identical N₂O records, and we average them to get our SH IAV signal with the same processing as for CO₂. The QBO circulation is known to reach throughout the stratosphere and into the troposphere (Tung and Yang, 1994; Hamilton and Fan, 2000), and multi-model studies have attributed the surface N₂O IAV to the STE flux (Ruiz et al., 2021). We can thus scale the surface N₂O IAV with the ratio of STE fluxes (CO₂:N₂O) to give an observational estimate of the STE-driven CO₂ IAV in the SH extra-tropics (dashed blue line in Figure 1d). The IAV in SH (40° S – 90° S) surface CO₂

calculated from the sCO₂ model scenario is also shown (dashed red line in Figure 1d). The modeled sCO₂ and observed N₂O-scaled IAVs are not always in phase, but they are in strong agreement in terms of amplitude: the STE IAV in CO₂ is a small fraction of the observed IAV. In addition, the modeled eCO₂ IAV shows that tropospheric circulation changes produce small IAV.

We compare CO₂ with well known interannual cycles in the Earth system in Figure 1d by plotting: (i) the QBO phase change (from easterly to westerly zonal equatorial wind at 40 hPa, see Newman, 2021) as thick gray vertical bars; and (ii) the times of moderate to extreme El Niños (red stars) and La Niñas (blue stars) (Trenberth, 2021). From this analysis, we expect minimal contribution of the QBO-driven circulation to the CO₂ IAV, and find no obvious connection between the two in this figure. For the El Niño–Southern Oscillation (ENSO), this simple comparison is inadequate. At best it shows that some of the larger positive SH IAV align with El Niños; whereas we know that ENSO affects ocean upwelling and continental rainfall and the CO₂ anomalies correlate very well with tropical ocean temperatures (Wang et al., 2021; Keeling and Graven, 2021).

3. Conclusions, Speculations, and Digressions

We have shown that the STE fluxes of old stratospheric air with "depleted" CO₂ have little influence on the IAV or annual cycles of CO₂ at the surface. The IAV observed for SH stations has a standard deviation of 0.22 to 0.28 ppm, while that for sCO₂ is at most 0.02 ppm in both hemispheres, that for eCO₂ is less than 0.02 ppm for SPO to SMO, and that for scaled-N₂O is 0.03 ppm for SPO+CGO average. The standard deviation for NH CO₂ IAV is larger, 0.4 to 0.6 ppm, and thus even less influenced by stratospheric air. Thus the speculations of Gaubert et al. (2019) regarding atmospheric transport can be dismissed.

The latitudinal pattern of N₂O IAV provides evidence for causes: e.g., the STE-driven signal weakens in the tropics and changes phase in the NH; and QBO composites show a clear separation of hemispheric sources (Ruiz et al., 2021). The latitudinal pattern of CO₂ IAV may similarly provide information on its cause. Comparing tropics to extra-tropics in the SH (SPO+CGO vs. SMO, solid and dotted black lines in Figure 1d), we find remarkably similar patterns after 1990, with similar amplitudes and some phase shifts of at most 1 year. If we add the NH tropics MLO IAV (not shown), the pattern and amplitude are similar. When the sites are in synch, one can only presume that the CO₂ perturbation is tied to changes in the growth/decay of tropical biomass transported equally to both hemispheres (Keeling and Graven, 2021). The challenge lies in the phasing and which region leads or lags in change. Unfortunately, the band-pass IAVs in this analysis do not seem able to accurately determine the phase at a level up to 1 year.

The Samoan site SMO provides a valuable but very challenging record of CO₂ and other trace gases having dominant NH emissions, such as chlorofluorocarbons (Cunnold et al., 1994) and N₂O (Nevison et al., 2007). Sometimes SMO is synchronous with the SH extra-tropics (CGO and SPO, which are almost always synchronous with each other) and at other times it links with MLO and the NH. Thus, to use SMO CO₂ as a metric for carbon cycle models, one must recognize that SMO is not simply representative of the SH tropics. When evaluating carbon cycle models, one should test tracer transport using the IAV for SMO versus SPO+CGO. As shown in Figure 1d, there are clear times when SMO is distinct from CGO+SPO (e.g., 1994, 1999, 2008 2012, 2015). At these times the SMO IAV matches that of MLO (not shown). These interannual shifts provide an excellent test for CO₂ historical simulations using weather

forecasting systems (e.g., McNorton et al., 2020) and realistic sources and sinks (e.g., Piao et al., 2018; Wang et al., 2020).

185

The rate of increase of the amplitude of the annual cycle of CO₂ is a key measure of changes in the biospheric and oceanic carbon cycles. The amplitude can be measured from the variance across 12 months. If the cycle is sinusoidal, then the max-min amplitude is equal to twice the square root of 2 times the standard deviation as plotted in Figure 1e.. With this approximation, we calculate a mean amplitude
190 of 17.0, 6.4, 1.3, 1.2, and 1.3 ppm for BRW, MLO, SMO, CGO, and SPO, respectively. These results are almost identical to those from the composited annual cycles (Figure 1b), but disagree at SMO as might be expected because of its double-peaked cycle. A linear fit to the standard deviations gives trends for the period 1985-2020 of 1.06 ± 0.15 , 0.142 ± 0.075 , 0.082 ± 0.047 , 0.079 ± 0.051 , and 0.031 ± 0.050 ppm decade⁻¹ for BRW, MLO, SMO, CGO, and SPO, respectively. The standard errors quoted here come from a
195 standard linear fit of the monthly values shown in Figure 1e, but are calculated more conservatively using 35 years as the degrees of freedom instead of 420 months. Our results for BRW and MLO agree well with other more extensive data analyses (Graven et al., 2013; Zhao and Zeng, 2014; Wenzel et al., 2016; Piao et al., 2018; Wang et al., 2020) but are able to identify emergent trends in the SH, which is not often used for model evaluation. A more serious uncertainty analysis focusing on the SH sources and sinks, the
200 annual and IAV cycles, and their trends would help solidify our knowledge of the carbon cycle.

Code and Data availability. All data and code used in this analysis are placed in the archive at
205 datadryad.org: 10.7280/D1N10J. The CTM code is in FORTRAN, and the post analysis code is in Matlab. All figures and their tabulated data are included.

Competing interests: The author declares no conflict of interest.

210 **Acknowledgements.** The author is grateful for the efforts of the reviewers and their insight, particularly in catching the problems and vagaries with band-pass filtering; the paper is much improved. I thank Ed Dlugokencky and his colleagues at the NOAA GML Carbon Cycle Cooperative Global Air Sampling Network for maintaining high quality, readily accessible data. I also acknowledge the support and assistance of my research group at UC Irvine, particularly Xin Zhu for the CTM simulations and Daniel
215 Ruiz for the N₂O simulations.

Financial support. The research at UCI has been supported by grants from the National Aeronautics and Space Administration's Atmospheric Chemistry Modeling and Analysis Program (ACMAP; grant no. 80NSSC21K1454), and the National Science Foundation's Atmospheric Chemistry Program (grant no. AGS-2135749).
220

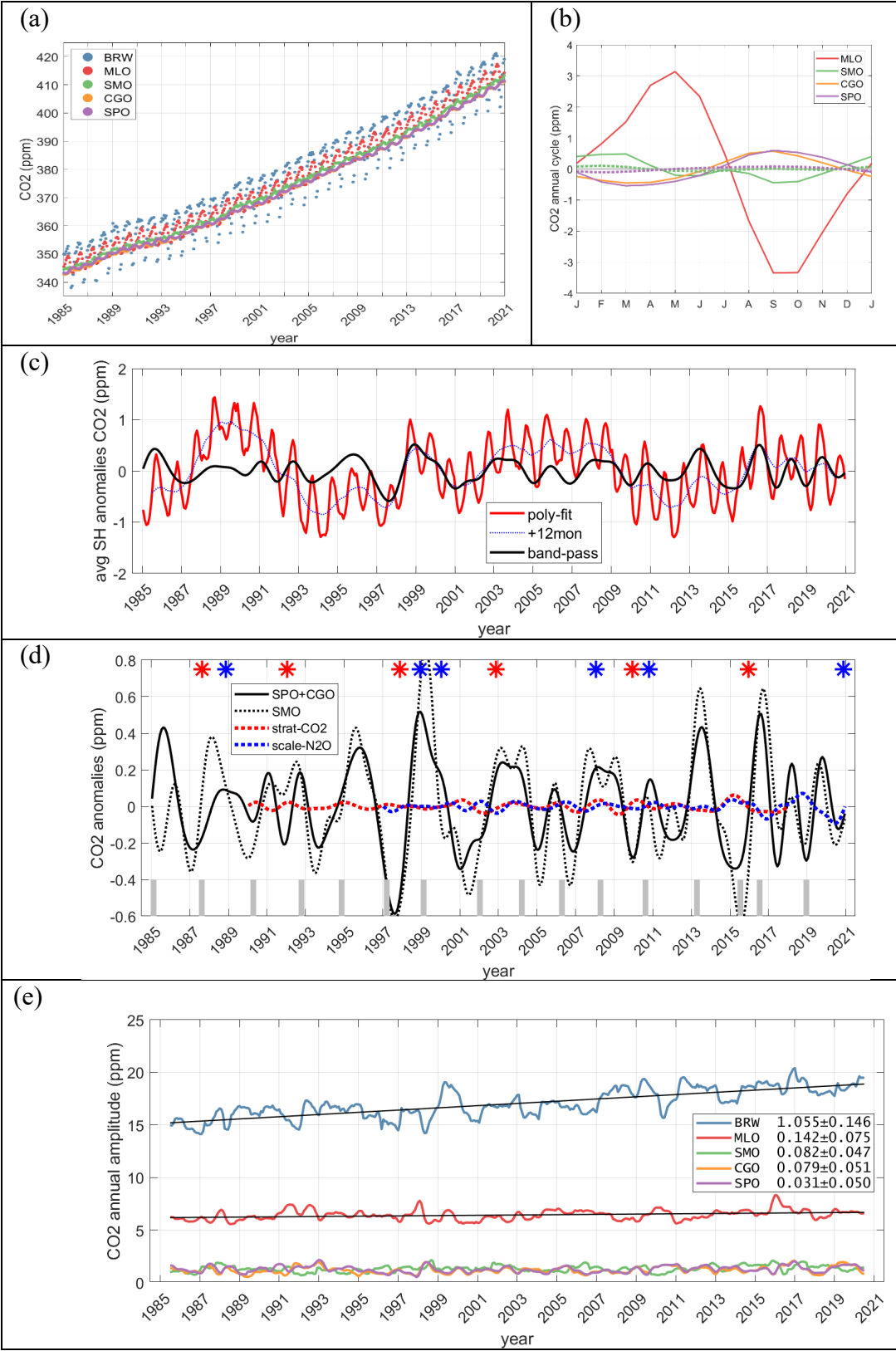
References

- 225 Baker, D. F., Law, R. M., Gurney, K. R., Rayner, P., Peylin, P., Denning, A. S., Bousquet, P., Bruhwiler, L., Chen, Y. H., Ciais, P., Fung, I. Y., Heimann, M., John, J., Maki, T., Maksyutov, S., Masarie, K., Prather, M., Pak, B., Taguchi, S., and Zhu, Z.: TransCom 3 inversion intercomparison: Impact of transport model errors on the interannual variability of regional CO₂ fluxes, 1988-2003, *Global Biogeochem Cy*, 20, Artn Gb1002, 10.1029/2004gb002439, 2006.
- Cunnold, D. M. Fraser, P. J. Weiss, R. F. Prinn, R. G. Simmonds, P. G. Miller, B. R. Alyea, F. N. and Crawford, A. J.: Global trends and annual releases of CCl₃F and CCl₂F₂ estimated from ALE/GAGE and other measurements from July 1978 to June 1991, *J. Geophys. Res.*, 99(D1), 1107-1126, doi: 10.1029/93JD02715, 1994.
230
- Deng, F., Jones, D. B. A., Walker, T. W., Keller, M., Bowman, K. W., Henze, D. K., Nassar, R., Kort, E. A., Wofsy, S. C., Walker, K. A., Bourassa, A. E., and Degenstein, D. A.: Sensitivity analysis of the potential impact of discrepancies in

- stratosphere–troposphere exchange on inferred sources and sinks of CO₂, *Atmos. Chem. Phys.*, 15, 11773–11788, doi: 10.5194/acp-15-11773-2015, 2015.
- 235 Dlugokencky, E.J., Crotwell, A.M., Mund, J.W., Crotwell, M.J., and Thoning, K.W.: Atmospheric Nitrous Oxide Dry Air Mole Fractions from the NOAA GML Carbon Cycle Cooperative Global Air Sampling Network, 1997-2020, Version: 2021-07-30, doi: 10.15138/53g1-x417, 2021b.
- Dlugokencky, E.J., Mund, J.W., Crotwell, A.M., Crotwell, M.J., and Thoning, K.W.: Atmospheric Carbon Dioxide Dry Air Mole Fractions from the NOAA GML Carbon Cycle Cooperative Global Air Sampling Network, 1968-2020, Version: 2021-07-30, doi: 10.15138/wkgj-f215, 2021a.
- 240 Engelen, R. J., Denning, A. S., Gurney, K. R., Law, R. M., Denning, A. S., Rayner, P. J., Baker, D., Bousquet, P., Bruhwiler, L., Chen, Y. H., Ciais, P., Fan, S., Fung, I. Y., Gloor, M., Heimann, M., Higuchi, K., John, J., Maki, T., Maksyutov, S., Masarie, K., Peylin, P., Prather, M., Pak, B. C., Sarmiento, J., Taguchi, S., Takahashi, T., and Yuen, C. W.: On error estimation in atmospheric CO₂ inversions, *J. Geophys. Res.-Atmos.*, 111, ArtD14199, doi: 10.1029/2006jd007428, 2006.
- 245 Frankenberg, C., Kulawik, S. S., Wofsy, S. C., Chevallier, F., Daube, B., Kort, E. A., O'Dell, C., Olsen, E. T., and Osterman, G.: Using airborne HIAPER Pole-to-Pole Observations (HIPPO) to evaluate model and remote sensing estimates of atmospheric carbon dioxide, *Atmos. Chem. Phys.*, 16, 7867–7878, doi: 10.5194/acp-16-7867-2016, 2016.
- Gaubert, B., Stephens, B. B., Basu, S., Chevallier, F., Deng, F., Kort, E. A., Patra, P. K., Peters, W., Rödenbeck, C., Saeki, T., Schimel, D., Van der Laan-Luijkx, I., Wofsy, S., and Yin, Y.: Global atmospheric CO₂ inverse models converging on neutral tropical land exchange, but disagreeing on fossil fuel and atmospheric growth rate, *Biogeosciences*, 16, 117–134, doi: 10.5194/bg-16-117-2019, 2019.
- 250 Graven, H. D., Keeling, R. F., Piper, S. C., Patra, P. K., Stephens, B. B., Wofsy, S. C., Welp, L. R., Sweeney, C., Tans, P. P., Kelley, J. J., Daube, B. C., Kort, E. A., Santoni, G. W., and Bent, J. D.: Enhanced Seasonal Exchange of CO₂ by Northern Ecosystems Since 1960, *Science*, 341, 1085-1089, 10.1126/science.1239207, 2013.
- 255 Gurney, K. R., Law, R. M., Denning, A. S., Rayner, P. J., Baker, D., Bousquet, P., Bruhwiler, L., Chen, Y. H., Ciais, P., Fan, S., Fung, I. Y., Gloor, M., Heimann, M., Higuchi, K., John, J., Maki, T., Maksyutov, S., Masarie, K., Peylin, P., Prather, M., Pak, B. C., Randerson, J., Sarmiento, J., Taguchi, S., Takahashi, T., and Yuen, C. W.: Towards robust regional estimates of CO₂ sources and sinks using atmospheric transport models, *Nature*, 415, 626-630, 10.1038/415626a, 2002.
- 260 Hamilton, K., and Fan, S. M.: Effects of the stratospheric quasi-biennial oscillation on long-lived greenhouse gases in the troposphere, *J. Geophys. Res.-Atmos.*, 105, 20581-20587, doi: 10.1029/2000jd900331, 2000.
- Keeling, R.F. and Graven, H.D.: Insights from Time Series of Atmospheric Carbon Dioxide and Related Tracers, *Annu. Rev. Environ. Resour.* 2021. 46:85–110, 10.1146/annurev-environ-012220-125406, 2021.
- 265 Koren, G., Schneider, L., van der Velde, I. R., van Schaik, E., Gromov, S. S., Adnew, G. A., Martino, D. J. M., Hofmann, M. E. G., Liang, M. C., Mahata, S., Bergamaschi, P., van der Laan-Luijkx, I. T., Krol, M. C., Rockmann, T., and Peters, W.: Global 3-D Simulations of the triple oxygen isotope signature delta O-17 in atmospheric CO₂, *J. Geophys. Res.-Atmos.*, 124, 8808-8836, doi: 10.1029/2019JD030387, 2019.
- Laskar, A. H., Mahata, S., Bhattacharya, S. K., and Liang, M. C.: Triple oxygen and clumped isotope compositions of CO₂ in the middle troposphere, *Earth Space Sci.*, 6, 1205-1219, doi: 10.1029/2019EA000573, 2019.
- 270 Le Quéré, C., Andrew, R. M., Canadell, J. G., Sitch, S., Korsbakken, J. I., Peters, G. P., Manning, A. C., Boden, T. A., Tans, P. P., Houghton, R. A., Keeling, R. F., Alin, S., Andrews, O. D., Anthoni, P., Barbero, L., Bopp, L., Chevallier, F., Chini, L. P., Ciais, P., Currie, K., Delire, C., Doney, S. C., Friedlingstein, P., Gkritzalis, T., Harris, I., Hauck, J., Haverd, V., Hoppema, M., Klein Goldewijk, K., Jain, A. K., Kato, E., Körtzinger, A., Landschützer, P., Lefèvre, N., Lenton, A., Lienert, S., Lombardozi, D., Melton, J. R., Metz, N., Millero, F., Monteiro, P. M. S., Munro, D. R., Nabel, J. E. M. S., Nakaoka, S., O'Brien, K., Olsen, A., Omar, A. M., Ono, T., Pierrot, D., Poulter, B., Rödenbeck, C., Salisbury, J., Schuster, U., Schwinger, J., Séférian, R., Skjelvan, I., Stocker, B. D., Sutton, A. J., Takahashi, T., Tian, H., Tilbrook, B., van der Laan-Luijkx, I. T., van der Werf, G. R., Viovy, N., Walker, A. P., Wiltshire, A. J., and Zaehle, S.: Global Carbon Budget 2016, *Earth Syst. Sci. Data*, 8, 605–649, doi: 10.5194/essd-8-605-2016, 2016.
- 275 Le Quéré, C., Andrew, R. M., Friedlingstein, P., Sitch, S., Pongratz, J., Manning, A. C., Korsbakken, J. I., Peters, G. P., Canadell, J. G., Jackson, R. B., Boden, T. A., Tans, P. P., Andrews, O. D., Arora, V. K., Bakker, D. C. E., Barbero, L., Becker, M., Betts, R. A., Bopp, L., Chevallier, F., Chini, L. P., Ciais, P., Cosca, C. E., Cross, J., Currie, K., Gasser, T., Harris, I., Hauck, J., Haverd, V., Houghton, R. A., Hunt, C. W., Hurtt, G., Ilyina, T., Jain, A. K., Kato, E., Kautz, M., Keeling, R. F., Klein Goldewijk, K., Körtzinger, A., Landschützer, P., Lefèvre, N., Lenton, A., Lienert, S., Lima, I., Lombardozi, D., Metz, N., Millero, F., Monteiro, P. M. S., Munro, D. R., Nabel, J. E. M. S., Nakaoka, S., Nojiri, Y., Padin, X. A., Pregon, A., Pfeil, B., Pierrot, D., Poulter, B., Rehder, G., Reimer, J., Rödenbeck, C., Schwinger, J., Séférian, R., Skjelvan, I., Stocker, B. D., Tian, H., Tilbrook, B., Tubiello, F. N., van der Laan-Luijkx, I. T., van der Werf, G. R., van Heuven, S., Viovy, N., Vuichard, N., Walker, A. P., Watson, A. J., Wiltshire, A. J., Zaehle, S., and Zhu, D.: Global Carbon Budget 2017, *Earth Syst. Sci. Data*, 10, 405–448, doi: 10.5194/essd-10-405-2018, 2018.
- 285 Liang, M. C., Mahata, S., Laskar, A. H., Thiemens, M. H., and Newman, S.: Oxygen isotope anomaly in tropospheric CO₂ and implications for CO₂ residence time in the atmosphere and gross primary productivity, *Sci. Rep.-UK*, 7, ArtD13180, doi: 10.1038/S41598-017-12774-W, 2017.
- 290 McNorton, J. R., Bousserez, N., Agusti-Panareda, A., Balsamo, G., Choulga, M., Dawson, A., Engelen, R., Kipling, Z., and Lang, S. M.: Representing model uncertainty for global atmospheric CO₂ flux inversions using ECMWF-IFS-46R1, *Geosci Model Dev*, 13, 2297-2313, 10.5194/gmd-13-2297-2020, 2020.

- 295 Nakazawa, T.: Current understanding of the global cycling of carbon dioxide, methane, and nitrous oxide, *Proc. Jpn. Acad. Ser. B Phys. Biol. Sci.* 96(9), 394–419, doi: 10.2183/pjab.96.030, 2020.
- Nassar, R., Jones, D. B. A., Kulawik, S. S., Worden, J. R., Bowman, K. W., Andres, R. J., Suntharalingam, P., Chen, J. M., Brenninkmeijer, C. A. M., Schuck, T. J., Conway, T. J., and Worthy, D. E.: Inverse modeling of CO₂ sources and sinks using satellite observations of CO₂ from TES and surface flask measurements, *Atmos. Chem. Phys.*, 11, 6029–6047, doi: 10.5194/acp-11-6029-2011, 2011.
- 300 Nevison, C. D., Kinnison, D. E., and Weiss, R. F.: Stratospheric influences on the tropospheric seasonal cycles of nitrous oxide and chlorofluorocarbons, *Geophys. Res. Lett.*, 31, L20103, <https://doi.org/10.1029/2004gl020398>, 2004.
- Nevison, C. D., Mahowald, N. M., Weiss, R. F., and Prinn, R. G.: Interannual and seasonal variability in atmospheric N₂O, *Global Biogeochem. Cycles*, 21, GB3017, doi:10.1029/2006GB002755, 2007.
- 305 Nevison, C. D., Dlugokencky, E., Dutton, G., Elkins, J. W., Fraser, P., Hall, B., Krummel, P. B., Langenfelds, R. L., O'Doherty, S., Prinn, R. G., Steele, L. P., and Weiss, R. F.: Exploring causes of interannual variability in the seasonal cycles of tropospheric nitrous oxide, *Atmos. Chem. Phys.*, 11, 3713–3730, <https://doi.org/10.5194/acp-11-3713-2011>, 2011.
- Newman, P.: The quasi-biennial oscillation (QBO), NASA, Goddard Space Flight Center, Retrieved from https://acd-ext.gsfc.nasa.gov/Data_services/met/qbo/qbo.html on 30 Aug 2021, 2021
- 310 Pandey, S., Houweling, S., Krol, M., Aben, I., Chevallier, F., Dlugokencky, E. J., Gatti, L. V., Gloor, E., Miller, J. B., Detmers, R., Machida, T., and Röckmann, T.: Inverse modeling of GOSAT-retrieved ratios of total column CH₄ and CO₂ for 2009 and 2010, *Atmos. Chem. Phys.*, 16, 5043–5062, doi: 10.5194/acp-16-5043-2016, 2016.
- Peylin, P., Law, R. M., Gurney, K. R., Chevallier, F., Jacobson, A. R., Maki, T., Niwa, Y., Patra, P. K., Peters, W., Rayner, P. J., Rödenbeck, C., van der Laan-Luijkx, I. T., and Zhang, X.: Global atmospheric carbon budget: results from an ensemble of atmospheric CO₂ inversions, *Biogeosciences*, 10, 6699–6720, 10.5194/bg-10-6699-2013, 2013.
- 315 Piao, S. L., Liu, Z., Wang, Y. L., Ciais, P., Yao, Y. T., Peng, S., Chevallier, F., Friedlingstein, P., Janssens, I. A., Penuelas, J., Sitch, S., and Wang, T.: On the causes of trends in the seasonal amplitude of atmospheric CO₂, *Global Change Biol.*, 24, 608–616, 10.1111/gcb.13909, 2018.
- Piao, S., Wang, X., Wang, K., Li, X., Bastos, A., Canadell, J. G., Ciais, P., Friedlingstein, P., and Sitch, S.: Interannual variation of terrestrial carbon cycle: Issues and perspectives. *Global Change Biology*, 26(1), 300–318. 10.1111/gcb.14884, 2020
- 320 Ray, E. A., Portmann, R. W., Yu, P. F., Daniel, J., Montzka, S. A., Dutton, G. S., Hall, B. D., Moore, F. L., and Rosenlof, K. H.: The influence of the stratospheric Quasi-Biennial Oscillation on trace gas levels at the Earth's surface, *Nat. Geosci.*, 13, 22, doi: 10.1038/s41561-019-0507-3, 2020.
- Ruiz, D. J. and Prather, M. J.: From the middle stratosphere to the surface, using nitrous oxide to constrain the stratosphere–troposphere exchange of ozone, *Atmos. Chem. Phys.*, 22, 2079–2093, <https://doi.org/10.5194/acp-22-2079-2022>, 2022.
- 325 Ruiz, D. J., Prather, M. J., Strahan, S. E., Thompson, R. L., Froidevaux, L., and Steenrod, S. D.: How atmospheric chemistry and transport drive surface variability of N₂O and CFC-11, *J. Geophys. Res.-Atmos.*, 126, ARTN e2020JD033979, doi: 10.1029/2020JD033979, 2021.
- Tang, Q., Prather, M. J., Hsu, J., Ruiz, D. J., Cameron-Smith, P. J., Xie, S., and Golaz, J.-C.: Evaluation of the interactive stratospheric ozone (O₃v2) module in the E3SM version 1 Earth system model, *Geosci. Model Dev.*, 14, 1219–1236, doi: 10.5194/gmd-14-1219-2021, 2021.
- 330 Trenberth, K. and National Center for Atmospheric Research Staff (Eds). Last modified 21 Jan 2020. "The Climate Data Guide: Nino SST Indices (Nino 1+2, 3, 3.4, 4; ONI and TNI)." Retrieved from <https://climatedataguide.ucar.edu/climate-data/nino-sst-indices-nino-12-3-34-4-oni-and-tni> on 1 June 2021, 2021.
- 335 Tung, K. K., and Yang, H.: Global QBO in circulation and ozone 2. A simple mechanistic model, *J. Atmos. Sci.*, 51, 2708–2721, doi: 10.1175/1520-0469(1994)051<2708:Gqicao>2.0.Co;2, 1994.
- Wang, K., Wang, X. H., Piao, S. L., Chevallier, F., Mao, J. F., Shi, X. Y., Huntingford, C., Bastos, A., Ciais, P., Xu, H., Keeling, R. F., Pacala, S. W., and Chen, A. P.: Unusual characteristics of the carbon cycle during the 2015–2016 El Niño, *Global Change Biol.*, 27, 3798–3809, 10.1111/gcb.15669, 2021.
- 340 Wang, K., Wang, Y. L., Wang, X. H., He, Y., Li, X. Y., Keeling, R. F., Ciais, P., Heimann, M., Peng, S. S., Chevallier, F., Friedlingstein, P., Sitch, S., Buermann, W., Arora, V. K., Haverd, V., Jain, A. K., Kato, E., Lienert, S., Lombardozi, D., Nabel, J. E. M. S., Poulter, B., Vuichard, N., Wiltshire, A., Zeng, N., Zhu, D., and Piao, S. L.: Causes of slowing-down seasonal CO₂ amplitude at Mauna Loa, *Global Change Biol.*, 26, 4462–4477, 10.1111/gcb.15162, 2020.
- Wenzel, S., Cox, P. M., Eyring, V., and Friedlingstein, P.: Projected land photosynthesis constrained by changes in the seasonal cycle of atmospheric CO₂, *Nature*, 538, 499–501, 10.1038/nature19772, 2016.
- 345 Zhao, F., and Zeng, N.: Continued increase in atmospheric CO₂ seasonal amplitude in the 21st century projected by the CMIP5 Earth system models, *Earth Syst Dynam.*, 5, 423–439, 10.5194/esd-5-423-2014, 2014.

350



355 **Figure 1 (a):** NOAA surface CO₂ monthly data (ppm, mole fraction) from Dlugokencky et al. (2021a). The 5 sites are: BRW = Barrow AK, 71°N, 156°W; MLO = Mauna Loa HI, 20°N, 156°W; SMO = Tutuila, Am. Samoa, 14°S, 171°W; CGO = Cape Grim, Tasmania, Australia, 41°S, 144°E; SPO = South Pole, 90°S. Monthly average in situ observations are used with gaps filled by flask data at the same site. Only one point is interpolated (SMO, May 2015). CGO is flask only.

360 **(b):** Mean annual cycle in surface CO₂ (ppm) at 4 sites (BRW not shown) using 1985 through 2021 calculated from the residuals after the polynomial fit was removed. The eCO₂ model results are shown as dotted lines for SMO and SPO with the same color coding; eCO₂ has similar phasing at SPO and is double-peaked at SMO, but the amplitudes (~0.18 ppm) are much smaller than observed. The sCO₂ amplitude is even smaller (~0.06 ppm) and not shown.

365 **(c):** Observed CO₂ variability (ppm) derived from the monthly averages of two SH extra-tropical stations (SPO and CGO) for the period 1985–2021. The poly-fit (solid red curve) shows the residuals after removal of a polynomial fit (average of 3rd and 4th order in time). A 12-month running mean (thin dashed blue curve) is derived from the poly-fit residuals and removes the annual cycle. The interannual variability (IAV, solid black curve) is derived from band-pass filtering described in the text. The band-pass limits [0.20 0.80] are set to truncate periods longer than 5 y and shorter than 1.25 y.

370 **(d):** Surface CO₂ IAV (ppm) for SH extra-tropics. The SPO+CGO IAV (black solid line) is compared with the SMO IAV (thin dotted black line). Other IAVs shown are: (1) model calculated sCO₂ (dashed red line) from the stratosphere-driven influx of aged, low-CO₂ air; and (2) N₂O observed IAV (dashed blue line) scaled to match flux of low-CO₂ air. The timing of the QBO phase change in equatorial zonal wind at 40 hPa from negative (easterlies) to positive (westerlies) is denoted with thick vertical gray bars. The timing of moderate to extreme El Ninos (red stars) and La Ninas (blue stars) are also shown.

375 **(e):** CO₂ annual amplitude (ppm, max-min) derived from the variance across 12 monthly values. Each monthly point (centered on the beginning of each month) is the standard deviation of the surrounding ±6 monthly means, scaled by $2\sqrt{2}$ to give the max-min amplitude as if it were a sine curve. The line fits for BRW and MLO are shown. The slope and standard error (SE) in units of ppm per decade are given in the legend. The SE is calculated conservatively based on the number of years rather than the number of months.

380